Available online at www.sciencedirect.com
ScienceDirect
Journal of the European Ceramic Society 30 (2010) 1351–1357
www.elsevier.com/locate/jeurceramsoc

Microstructure development, hardness, toughness and creep behaviour of pressureless sintered alumina/SiC micro–nanocomposites obtained by slip-casting

H. Reveron *, O. Zaafrani, G. Fantozzi

Université de Lyon, Insa-Lyon, MATEIS CNRS UMR 5510, 20 Av. Albert Einstein, F-69621, Villeurbanne Cedex, France

Received 18 July 2009; received in revised form 7 October 2009; accepted 27 November 2009
Available online 12 January 2010

Abstract

Al_2O_3–SiC micro–nanocomposites are much more resistant materials than monolithic alumina regarding some mechanical properties. In order to study the possibility of obtaining creep resistant alumina/SiC micro–nanocomposites using inexpensive forming methods, alumina 1 and 5 vol% SiC materials were produced by slip-casting and pressureless sintering. Well-densified alumina–SiC pressureless sintered materials were obtained at 1700 °C for 2 h and attained 97–99% of the theoretical density. The microstructure, hardness and toughness were examined and 4-point flexure creep tests were performed at 1200 °C and 100 MPa in air. Compared with pure alumina materials, the creep resistance, toughness and hardness were enhanced drastically in materials containing 5 vol% of SiC.

Keywords: Ceramic matrix composites (CMC); Forming processes; Sintering; Microstructure; Creep; Hardness; Toughness

1. Introduction

Since the first time that the concept of "ceramic nanocomposites" was introduced by Niihara, 1991,[1] worldwide researchers have been trying to optimize the microstructure of this type of materials, expecting an improvement in their performances. The concept of nanocomposites, that involves the incorporation of some fine particles into a host matrix, has been applied successfully in many ceramic systems which have already developed better mechanical properties (strength, hardness, toughness and creep resistance).

Two types of nanocomposite microstructures have been described by Niihara: (1) "nano–nano" or a dispersion of two nanophases and (2) "micro–nano" or a dispersion of fine inclusions into a micro-sized matrix. Because the creep of ceramics shows a strong dependence on the gain size (the creep resistance decreases with the grain size), the so-called micro–nanocomposites are more suitable for creep applications. This is the reason why we are so interested in developing this type of microstructure. In this case, three subtypes of microstructures have been proposed in where nanoparticles could be located – only along the grain boundaries (intergranular type), – inside the grains (intragranular type), or—at all of these positions (intra-intergranular). Despite this subdivision and for the whole of "micro–nano" ceramic systems already produced, only the last type of microstructure has been reported in the literature.

The nanocomposite effect on alumina matrix was first demonstrate by Niihara and Nakahira[2] who reported an increase in the fracture strength and toughness from 350 MPa or 3 MPa$\sqrt{}$m in pure Al_2O_3 up to 1050 MPa or 4.7 MPa$\sqrt{}$m in composites with 5 vol% SiC nanoparticles. Following the initial work of Niihara, much interest was paid to the study of Al_2O_3–SiC nanocomposites properties which were prepared mainly using conventional power routes (powder mixing) and expensive hot-pressing (HP) or hot-isostatic-pressing (HIP) methods. Systems containing 5–25 vol% SiC nanopowder in a 1–5 μm micro-sized pure alumina matrix were extensively produced by these techniques in quest of matrix mechanical reinforcement.[3–6] However, the important increase in toughness and fracture strength firstly reported by Niihara could not be obtained again even if numerous studies have tried. If it is true that HP or HIPing techniques can contribute to overcome the problem of nanocomposite densi-

* Corresponding author.
E-mail address: helen.reveron@insa-lyon.fr (H. Reveron).

0955-2219/$ – see front matter © 2009 Elsevier Ltd. All rights reserved.
doi:10.1016/j.jeurceramsoc.2009.12.008

Table 1
Starting powders characteristics.

Material	Phase (%)	Purity (%)	BET particle size (nm)	Specific area (m^2/g)
Al_2O_3 *CR1*	95% α-Al_2O_3 5% γ-Al_2O_3	99.9	457	3.3
SiC *UF25*	α-SiC 6H/4H polytype	98.0	78	24.5

fication, a substantial increase of the production cost, especially when complex shapes are required, is expected.

The use of inexpensive methods such as slip-casting and conventional sintering in order to produce dense and homogeneous alumina–SiC nanocomposites has been reported very little. Moreover, we have not found any report on creep behaviour carried out in slip-casted and conventionally sintered materials. This is probably due because obtaining high densities become much more complicated by using conventional pressureless sintering. Only a few research works have been carried out on pressureless sintering of alumina–SiC nanocomposites formed by pressing (cold isostatic pressing or CIP), pressure filtration or gel casting. Among them we can cite the results reported by Borsa et al.[7] who produced pressed Al_2O_3–5 vol% SiC composites reaching 95.5% or 98.5% of the theoretical density at 1600 °C or 1700 °C respectively (Ar atmosphere; dwell time of 2 h), or by Stearns et al.[8] who sintered Al_2O_3–5 vol% SiC up to 98.3% at 1775 °C (N_2 atmosphere, dwell time of 4 h). For equivalent materials, nitrogen rather than argon makes it possible to promote alumina–SiC nanocomposites densification as has been shown by Anya and Roberts[9] in the case of CIP-ed 5 vol%SiC systems sintered until 99.8% under nitrogen or 98.2% under argon. Timms et al.[10] used the pressure filtration technique for forming Al_2O_3–5 vol%SiC nanocomposites with excellent green densities (64% from slurries containing 50 vol% solids loading) and near fully dense after pressureless sintering at 1900 °C (99% td). More recently, Ananthakumar et al.[11] have also employed a chemical route called gel casting to shape alumina–SiC nanocomposites but in this study sintering was only performed under 80 bar of gas pressure (1700 °C/2 h) to obtain 97% of the theoretical density.

In the present work, the possibility of obtaining dense and homogeneous micro–nano Al_2O_3–SiC composites (1 and 5 vol% SiC) by slip-casting and pressureless sintering is demonstrated. Besides the production cost reduction related to the sintering method, the use of the slip-casting technique avoids the step of slurry drying which usually leads to the formation of hard agglomerates and then to the poor densities in the case of natural sintered pressed compacts, it also allows the processing of complex shapes. Moreover, comparing to forming by pressing, the safety of the whole processing was enhanced because SiC nanoparticles remained confined in a liquid phase during forming.

The effect of SiC containing on the creep behaviour, toughness and hardness of alumina-based materials obtained by slip-casting and pressureless sintering are discussed here based on microstructural features. As will be shown later, it is possible to obtain similar steady state creep rates in both materials developed here (1 and 5 vol% SiC) due to the effect of the matrix grain size. It is clear that a compromise must be found between the matrix grain size and the SiC content which enables to develop creep resistant materials exhibiting good mechanical properties at room temperature.

2. Experimental procedure

2.1. Starting materials and processing

As starting materials, a high purity Al_2O_3 powder (*CR1*, from Baikowski-France) with a very low amount of Mg (<1 ppm) and a SiC fine powder (*UF25* from Starck-Germany) were used. The main characteristics of the starting materials are listed in Table 1. A powder mixture composed of Al_2O_3 and SiC nanoparticles was ball-milled in distilled water for 40 h, using an anionic commercial dispersant (0.2 wt% of Darvan C with respect of solids), 50 wt% of solid loadings and zirconia balls as grinding media (2 mm in diameter). Two suspensions were obtained in this manner containing 1 vol% and 5 vol% SiC at basic pH (by adding NH_4OH). Another suspension was also prepared from alumina powder only under natural pH conditions.

After ball-milling, the slurries were degassed under vacuum for few minutes. The slurries were then slip-casted over Paris plaster moulds using polyethylene plates. Slip-cast samples were dried (24 h at ambient temperature and 48 h at 50 °C) and sintered under argon using a conventional graphite furnace. During the thermal treatment, debinding was performed at 1 °C/min up to 600 °C for 1 h (vacuum) and sintering by heating at 5 °C/min up to 1700 °C for 2 under argon atmosphere. The experimental materials are shown in Table 2.

2.2. Physical and structural characterization

After slip-casting and drying, green densities were estimated geometrically. Relative green densities for Al_2O_3–1 or 5 vol% of SiC materials were determined from theoretical densities by applying the rule of mixtures (3.968 g/cm^3 for alumina and 3.943 g/cm^3 for SiC).

Phase identification on sintered samples was performed by means of X-ray diffraction (XRD) using Ni-filtered Cu Kα radiation (0.1541 nm). The scanned angles were ranging between 20° and 80° (in 2θ scale) with a step width of 0.05° and an exposure time of 1 s (X-ray Bruker D8 diffractometer). Bulk density was determined by Archimedes method using distilled water and three different weight measurements (dried mass, mass in water and mass imbedded in water) according to the C373-88(2006) ASTM standard test method. The relative density was obtained by correlating the bulk density with the theoretical density of mixtures.

Table 2
The experimental materials.

Material	Td (%)	Matrix grain size (μm)	Inter SiC (%)	SiC inter size (nm)	SiC intra size (nm)	ZrO_2 inter size (nm)	ZrO_2 intra size (nm)	H_v (GPa)	K_{IC} Anstis ($MPa\,m^{1/2}$)	K_{IC} Liang ($MPa\,m^{1/2}$)
Al_2O_3	99.3	28.2 ± 12.8	–	–	–	–	–	15.1 ± 1.1	2.7 ± 0.4	3.6 ± 0.4
Al_2O_3–1 vol% SiC	99.2	12.7 ± 7.9	21% (0.21%)[a]	224 ± 142	105 ± 106	339 ± 95	309 ± 74	15.6 ± 1.0	3.4 ± 0.6	4.3 ± 0.6
Al_2O_3–5 vol% SiC	97.1	1.4 ± 0.4	58% (2.90%)[a]	243 ± 154	114 ± 63	649 ± 123	300 ± 60	16.4 ± 0.6	4.0 ± 0.7	5.2 ± 0.7

[a] Over the added SiC volume.

Microstructural features on sintered samples were examined by SEM (ESEM-FEG XL-30 FEI apparatus) on fractured and/or polished surfaces. After polishing, samples were thermally etched at 1400 °C for 1 h under argon atmosphere in order to reveal grain morphology. Several microstructural parameters (alumina and SiC grain sizes, SiC particles size distribution, zirconia pollution from grinding media) were extracted from SEM analysis. Grain sizes were estimated from at least 200 measurements.

2.3. Mechanical testing

Hardness and indentation fracture toughness were determined from Vickers impression marks. Vickers hardness was determined on polished surfaces with a load of 49 N (5 kg) applied for 10 s according to:

$$H = 1.8544\left(\frac{P}{d^2}\right) \tag{1}$$

where P is the load and d is the length of the impression diagonal. In each composite and pure alumina samples, at least 20 indentation imprints were made. The mean value and its standard deviation were then calculated.

The indentation fracture toughness (K_{IC}) was determined from indentation fracture lengths by applying two different equations. The first one proposed by Anstis et al.[12] for cracks of median type:

$$\sigma = 0.016\left(\frac{E}{H}\right)^{0.5}\left(\frac{P}{{c_o}^{3/2}}\right) \tag{2}$$

where E is the Young's modulus, H the Vickers hardness, c_o the crack length (measured by optical microscopy from the centre of indentation to the end of the crack). The second one which was developed by Liang et al.[13] which is more general because it works either for median or Palmqvist cracks:

$$\left(\frac{K_{IC}\phi}{Ha^{1/2}}\right)\left(\frac{H}{E\phi}\right)^{0.4}\alpha = \left(\frac{c_o}{a}\right)^{(c/18a)-1.51} \tag{3}$$

where E is the Young's modulus, ϕ is a constraint factor, α is a non-dimensional constant function of the Poisson's ration of the material taken for alumina as 390 MPa, 3 and 9.3 respectively. As in the Antis case, H is the measured Vickers hardness value, c_o the crack length and a the half-diagonal of the Vickers indentation imprint. A value of Young's modulus for nanocomposites was calculated using the rule of mixture with $E(Al_2O_3) = 390$ MPa and $E(SiC) = 414$ MPa.

Creep tests were carried out in air in a 4-point-bending fixture at 1200 °C and under 100 MPa, using a testing machine which has been developed at our laboratory. Samples for creep were parallelepipeds with the following dimensions: b (sample with) 4 mm, w (sample height) 3 mm and l (sample length) 40 mm. Prior to testing, tensile faces were polished with diamond paste down to 3 μm and the edges were chamfered (about 45°) in order to avoid the influence of micro-cracks on the creep behaviour. The 4-point bending fixture made from alumina has an outer and inner span of 36 mm and 18 mm respectively. For a fixed

temperature and load, the flexural stress on the tensile face of the specimen was calculated as follows:

$$\sigma = \frac{3P(L - L')}{2bw^2} \quad (4)$$

where P is the applied load, L the outer span, L' the inner span, b the sample width and w the sample height.

Hollenberg et al.[14] showed that the creep strain ε can be calculated from the deflection "y" at the centre of the specimen, if there is no major cracking in the specimen and the deflection remains small compared to the inner span L' as:

$$\varepsilon = K(n).y \quad (5)$$

with

$$K(n) = \frac{2w(n+2)}{(L - L\prime)[L + L\prime(n+1)] + L\prime^2(n+2)/2} \quad (6)$$

and n the creep stress exponent.

Furthermore, the steady-state creep rate $\dot{\varepsilon}$ can be expressed by the following equation:

$$\dot{\varepsilon} = A\frac{\sigma^n}{d^p}\exp\left(-\frac{Q}{RT}\right) \quad (7)$$

where A is a material constant, σ the applied stress, d the grain size, p the grain size exponent, Q the activation energy for creep, R the gas constant and T the absolute temperature.

From the $K(n)$ expression (see Eq. (6)), it is clear that this constant depends certainly on n but also on the outer and inner span. Nevertheless, when L/L' is close to 2, $K(n)$ becomes almost insensitive to the n value.[14] In this manner the creep rate ε can be calculated by using the expression (5) with a supposed n value. If determined and initial supposed n values are too different, calculations of ε must be realized again by setting another n value and so on.

3. Results and discussion

Table 2 give the values of density and matrix grain size obtained after pressureless sintering. Densification at 1700 °C for 2 h allowed densities >99% of full density in pure alumina and alumina–1 vol% SiC composite. The negative consequence of putting SiC nanoparticles on density is observed in samples containing 5 vol% SiC, where 97.1% of full density was reached.

The average matrix grain size decreased with SiC addition because of alumina grain boundary pinning effect. Such as in the work recently published by Dong et al.[6], a Zener-type model could be used to estimate matrix grain sizes satisfactorily from SiC composition ($D_{max} = 4r/3f$; where r is the radius of the secondary particles, and f its volume fraction). On the contrary, other previous experimental studies have shown that SiC pinning effect on alumina–SiC based materials cannot be predicted from equilibrium models (either Zener or topological models).[15,16]

Principal microstructural features regarding SiC nanoparticle sizes and positioning are also resumed in Table 2. Both alumina–SiC composites exhibit inter–intragranular-type microstructures which differ principally in the number of intergranular particles as shown in Fig. 1.

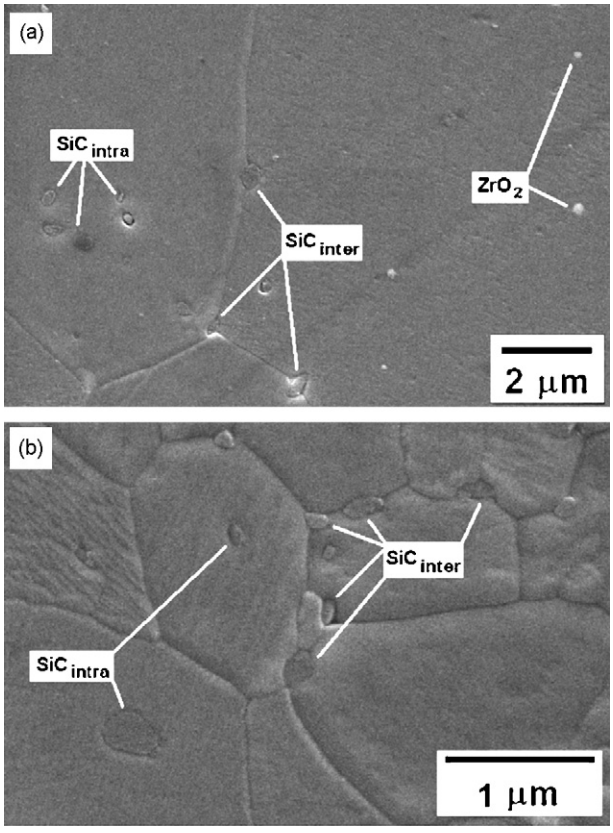

Fig. 1. SEM micrographs of polished and thermally etched surfaces of the different sintered alumina–SiC composites: (a) with 1 vol% SiC, (b) with 5 vol% SiC (1700 °C—2 h, white spots are ZrO_2 impurities from milling).

The fraction of SiC particles located at the grain boundaries (intergranular) was determined by counting at least 200 particles and following the procedure proposed by Stearns et al.[16] We estimated this fraction to be about 21% in the case of 1 vol% SiC (alumina grain size of 12.7 ± 7.9 μm) or 58% in the case of 5 vol% SiC (alumina grain size of 1.4 ± 0.4 μm). Moreover, SEM analysis showed up a relatively lower size of intragranular particles as previously reported in the literature. This fact is also in agreement with classical pinning models which propose that for immobile second-phase inclusions (pore or particles) the limitation of grain growth decreases as the effective size of inclusions decreases. In other words, bigger particles are more efficient in pinning grain boundaries and are usually found at intergranular positions.

X-ray diffraction patterns for alumina CR1 with 1 and 5 vol% SiC UF25 sintered samples are reported in Fig. 2.

After pressureless sintering at 1700 °C both ceramics are characterized by the presence of alpha alumina (JCPDS file 46-1212) and alpha-SiC crystallized under 6H polytype (JCPDS file 72-0018) and zirconia (JCPDS 49-1429). No detection of elemental aluminium or silicon was observed by XRD showing that no alumina/SiC reactions or SiC decomposition occurred during sintering due to the relatively low temperature (1700 °C). Effectively, Ihle et al.[17] have reported that temperatures as high as 1925 °C are required to have a reaction between SiC and alumina. The very low intense XRD zirconia peaks revealed grinding media damage during the ball-milling step.

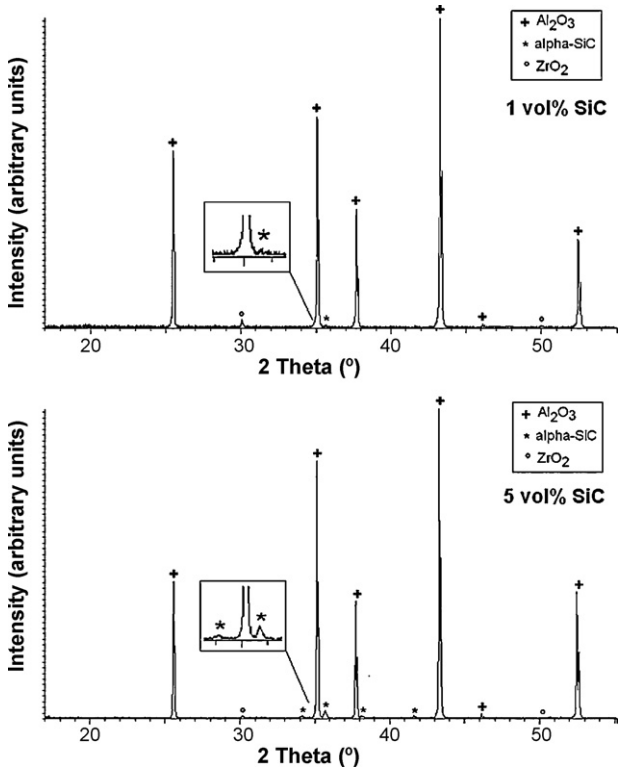

Fig. 2. X-ray diffraction analyses performed on alumina CR1–SiC UF25 sintered samples (1700 °C—2 h/Ar).

Because of the difference on SiC contents, by pressureless sintering we were able to develop two different composite microstructures which exhibited a coarse (12.7 ± 7.9 μm: 1 vol% SiC) and a fine (1.4 ± 0.4 μm: 5 vol% SiC) matrix grain size. Even with SiC additions of as low as 1 vol% SiC, a matrix grain size refinement was obtained (28.2 ± 12.8: 0% SiC for a sample prepared under the same conditions). Taking into account the fact that creep in alumina ceramics is strongly dominated by the grain size, the production of a coarse alumina matrix containing only 1 vol% SiC appears to be highly attractive for creep resistant applications as we will show by the following. In this case, we expect to have a relatively good creep resistance governed by the matrix grain size and a modest mechanical enhancement (hardness and toughness) which would be enough for a number of applications (see Table 2).

Fig. 3 shows results of creep tests at 1200 °C and under 100 MPa performed on sintered composites. Both curves exhibit only primary creep and steady-state creep region (no tertiary creep region was observed). Moreover, samples were not fractured after 50 h of test. We see that the total deformation and the steady-state deformation rate were lowered by a factor of 2 or 3 in the system containing low SiC amount.

For creep resistance (strain and strain rates) the incorporation of a low amount of SiC nanoparticles (1 vol% instead 5 vol%) which leads to a coarser alumina matrix containing some intergranular particles (21% of 1 vol%, that is 0.21 vol%) effectively is more favourable than a finer microstructure even if the number of SiC nanoparticles at intergranular positions in this last sample was highly enhanced (58% of 5 vol% or

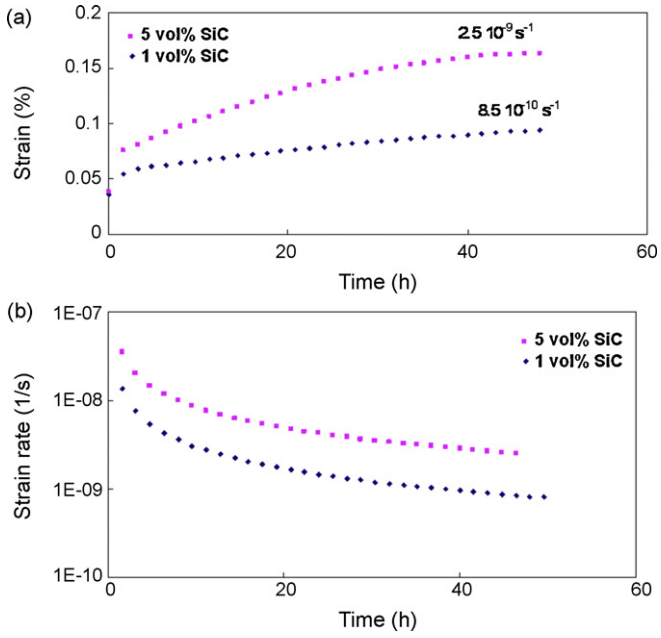

Fig. 3. Creep curves at 1200 °C and under 100 MPa for alumina/SiC composites: (a) strain and (b) strain rate.

2.9 vol%). This behaviour could be explained based on the two principal effects[18] which seem to be responsible for creep in alumina–SiC systems: (1) the SiC pinning effect by particles located at intergranular positions which is favourable to creep resistance because it decreases grain boundary sliding and enhances grain boundary strength and (2) the matrix grain growth inhibition caused by SiC particles which is unfavourable because as described above most mechanisms responsible of high-temperature creep in ceramics predict a steady-state creep rate which varies strongly with the grain size (more specifically with $1/dp$ where "d" is the grain size and p the grain size exponent, see Eq. (7)).

With the purpose of estimate more precisely the contribution of each effect on the creep properties of developed alumina—1 and 5 vol% SiC samples, we used both Nabarro-Herring and Coble models to obtain calculated creep rates as a function of alumina grain size at 1200 °C and 100 MPa.[19,20] For Nabarro-Herring model, the steady-state creep rate was estimated as follows[20]:

$$\dot{\varepsilon} = \frac{40\Omega_v D_1^+ \sigma}{2kTd^2} \tag{8}$$

where Ω_v is the atomic volume, $D_1{}^+$ is the coefficient for cation diffusion, σ is the applied stress, d is the grain size, k is Boltzmann's constant and T is the absolute temperature.

For Coble creep rate the following equation was employed:

$$\dot{\varepsilon} = \frac{48\Omega_v \delta D_{gb}^+ \sigma}{2kTd^3} \tag{9}$$

where δ is the effective width of the grain boundary for vacancy diffusion and $D_{gb}{}^+$ is the coefficient for grain-boundary cation diffusion. Both equations were evaluated for $d = 1.4$, 12.7 and 28.2 μm, $\Omega_v = 4.5 \times 10^{-29}$,

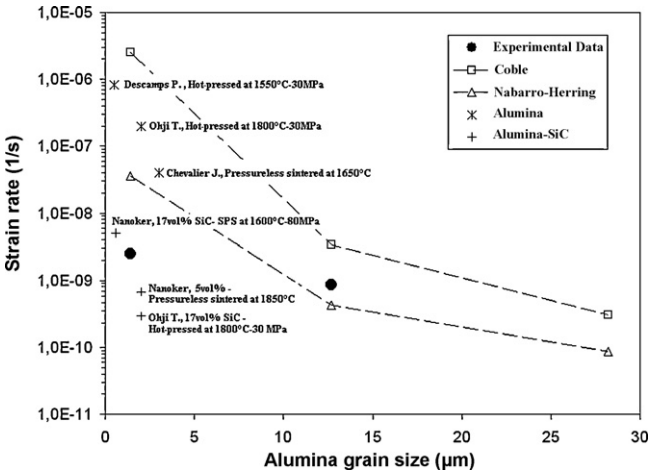

Fig. 4. Calculated alumina steady-state creep rates at 1200 °C and 100 MPa from Nabarro-Herring and Coble models. Steady state creep rates of 1 and 5 vol% SiC alumina composites are also displayed (black marks) and some already published experimental values from the literature.[4,18,21,22]

$T = 1473$ K, $D_1{}^+ = 2.8 \times 10^{-4} \exp(-478{,}000/8.3T)\ \mathrm{m^2\ s^{-1}}$ and $\delta D_{gb}{}^+ = 8.6 \times 10^{-10} \exp(-418{,}000/8.3T)\ \mathrm{m^3\ s^{-1}}$. Fig. 4 shows not only the calculated values for Nabarro-Herring and Coble creep (dashed lines) but also the creep rate data for 1 and 5 vol% alumina–SiC composites (black marks) and some experimental values extracted from past works done on pure alumina and alumina–SiC composites and tested under the same experimental conditions employed by us (flexural creep at 1200 °C and 100MPa-under air).

Inspection of Fig. 4 reveals that in the composite with the largest matrix grain size (1 vol% SiC), the steady-state creep rate is placed between the predicted Coble or Nabarro-Herring rates while in the composite having a small matrix grain size (5 vol% SiC), the strain rate falls considerably below both predicted rates either from Coble or Nabarro-Herring models.

Some works in the literature have proposed that alumina creep is predominantly dominated by aluminium grain boundary diffusion (Coble creep) if low grain sizes and relatively low testing temperatures are used. At larger grain sizes and higher temperatures, creep rates appears to be governed by a competition between lattice and grain boundary diffusion processes and Nabarro-Herring creep or a mixing of the two diffusional mechanisms have been already reported.[19,20,23] These previous observations are well supported by the three pure alumina points represented in Fig. 4. If only diffusional mechanisms are considered, it appears that creep behaviour in alumina–1 vol%SiC composites is almost entirely governed by the size of the matrix (rather than by the SiC addition) while in alumina–5 vol%SiC composites, the pinning effect is highly responsible in lowering the creep strain rate. All these observations confirm that microstructures features must be carefully tailored if highly creep resistance materials are required. In the case of micro–nanocomposites, not only the SiC content has to be controlled but also the matrix grain size. In this way, by using conventional sintering methods we obtained lower creep strain and strain rates by putting only some SiC nanoparticles into the alumina matrix (1 vol%) but sacrificing room temperatures properties such as hardness and toughness due to the coarse matrix grain size which was developed. As shown in Table 2, Vickers hardness and toughness values estimated from Vickers imprints showed a tendency for hardness and toughness increase with the SiC content.

Unfortunately, only few works[4,22] have been reported steady-state creep rates for alumina–SiC composites tested under the same conditions used in our work (see Fig. 4). Nonetheless, we observe that the creep resistance obtained on both alumina–SiC composites prepared through slip-casting and pressureless sintering at 1700 °C is located in the range of the previous works. Speaking of 5 vol% SiC composition, it seems that an increase on creep resistant could be obtained by sintering at high temperatures what would cause a little increase in the matrix grain size (more favourable for creep resistance). For the same matrix grain size, creep resistance appears to be improved by increasing the SiC addition as showed by Ohji et al.[4] who have reported the best creep rates up to date for alumina–17 vol% SiC composites.

4. Conclusions

Experimental results indicate that it is possible to produce highly dense and creep resistant alumina–SiC micro–nanocomposites by using inexpensive techniques such as slip-casting and pressureless sintering. Depending on the SiC composition, developed matrix grain sizes could be coarse (1 vol% SiC) or fine (5 vol% SiC) as a result of the SiC pinning effect described through a classical Zener-type model. Thereby, the volume of added SiC particles located at the grain boundaries was of only 0.21% (for 1 vol% SiC) and of 2.9% (for 5 vol% SiC). In both microstructures, large SiC particles were mainly located at the alumina grain boundaries (mean size 224–243 nm) and nearly all nanoparticles with mean size <105–114 nm were enclosed into alumina grains. Moreover, Vickers characterization showed a tendency for toughness and hardness increase with SiC addition.

Creep rate depends on the SiC composition because of the differences on the developed matrix grain size governed by the well-known pinning effect which operates during pressureless sintering. In samples with 1 vol% SiC, the excellent creep resistance appears to be governed by the size of the matrix while when 5 vol% SiC is added, an additional creep enhancement is obtained thank to SiC addition (SiC particles located at intergranular positions could contribute to reducing grain boundary sliding).

Further work on slip-casting and pressureless sintering of alumina–SiC materials obtained from a coarser alumina powder and/or finer SiC nanoparticles help us towards the preparation of a tailored microstructure, combining excellent mechanical properties either at room and high temperatures.

Acknowledgement

Financial support of this project by the European Commission is gratefully acknowledged (IP Nanoker NMP3-CT-2005-515784). The authors would like to thank Dr. Rajaa Benzaid for her help in creep experiments.

References

1. Niihara K. New design concept of structural ceramics–ceramic nanocomposites. *Centennial Memorial Issue of Ceram Soc Jpn* 1999;**99**:974–82.
2. Niihara K, Nakahira A. Strengthening and toughening mechanisms in nanocomposite ceramics. *Ann Chim Fr* 1991;**16**:479–86.
3. Zhao J, Stearns L, Harmer M, Chan H, Miller G. Mechanical behavior of alumina-silicon carbide "nanocomposites". *J Am Ceram Soc* 1993;**76**:503–10.
4. Ohji T, Hirano A, Nakahira K, Niihara K. Tensile creep behaviour of alumina/silicon carbide nanocomposite. *J Am Ceram Soc* 1994;**77**:3259–62.
5. Deng Z, Zhang Y, Shi J, Guo J. Microstructure and flexure creep behaviour of SiC-particle reinforced Al_2O_3 matrix composites. *J Eur Ceram Soc* 1996;**16**:1337–43.
6. Dong Y, Xu F, Shi X, Zhang C, Zhang Z, Yang J, et al. Fabrication and mechanical properties of nano-/micro-sized Al_2O_3/SiC composites. *Mater Sci Eng A* 2009;**504**:49–54.
7. Borsa C, Jiao S, Todd RAD, Brook R. Processing and properties of Al_2O_3–SiC nanocomposites. *J Microsc* 1995;**177**:305–12.
8. Stearns L, Zhao J, Harmer M. Processing and microsctructure development in Al_2O_3–SiC "nanocomposites". *J Eur Ceram Soc* 1992;**10**:473–7.
9. Anya C, Roberts S. Pressureless sintering and elastic constants of Al_2O_3–SiC nanocomposites. *J Eur Ceram Soc* 1997;**17**:565–73.
10. Timms L, Ponton C, Stranswood M. Processing of Al_2O_3/SiC nanocomposites. Part 2. green body formation and sintering. *J Eur Ceram Soc* 2002;**22**:1569–86.
11. Ananthakumar S, Prabhakaran K, Hareesh U, Manobar P, Warrier K. Gel casting for Al_2O_3–SiC nanocomposites and its creep characteristics. *Mater Chem Phys* 2004;**85**:151–7.
12. Anstis G, Chantikul P, Lawn B. A critical evaluation of indentation techniques for measuring fracture toughness. I. Direct crack measurements. *J Am Ceram Soc* 1981;**64**:533–8.
13. Liang K, Orange G, Fantozzi G. Evaluation by indentation of fracture toughness of ceramic materials. *J Mater Sci* 1990;**25**:207–14.
14. Hollenberg G, Terwilliger G, Gordon R. Calculation of stresses and strains in four-point bending creep tests. *J Am Ceram Soc* 1971;**54**: 196–9.
15. Wang H, Gao L, Guo J. The effect of nanoscale SiC particles on the microstructure of Al_2O_3 ceramics. *Ceram Int* 2000;**26**: 391–6.
16. Stearns L, Harmer M. Particle-inhibited grain growth in Al_2O_3–SiC. I. Experimental results. *J Am Ceram Soc* 1996;**79**:3013–9.
17. Ihle J, Herrmann M, Adler J. Phase formation in porous liquid phase sintered silicon carbide. Part I. Interaction between alumina and SiC. *J Eur Ceram Soc* 2005;**25**:987–95.
18. Descamps P, O'Sullivan D, Poorteman M, Descamps J, Leriche A, Cambier F. Creep behaviour of Al_2O_3–SiC nanocomposites. *J Eur Ceram Soc* 1999;**19**:2475–85.
19. Cannon R, Langdon T. Review creep of ceramics. *J Mater Sci* 1988;**23**:1–20.
20. Chokshi A, Porter J. High temperature mechanical properties of single phase alumina. *J Mater Sci* 1986;**21**:705–10.
21. Chevalier J, Olagnon C, Fantozzi G, Gros H. Creep behaviour of alumina, zirconia and zirconia-toughened alumina. *J Eur Ceram Soc* 1997;**17**:859–64.
22. IP-Nanoker report, 6th FP NMP3-CT-2005-515784, 2008.
23. Lessing P, Gordon R. Creep of polycrystalline alumina, pure and doped with transition metal impurities. *J Mater Sci* 1977;**12**:2291–302.